AN IMPROVED EFFECTIVE WIDTH METHOD BASED ON THE THEORY OF PLASTICITY

Thomas Hansen *, Jesper Gath and M.P. Nielsen

ALECTIA A/S, Teknikerbyen 34, DK-2830 Virum, Denmark
**(Corresponding author: E-mail: tmh@alectia.com)*

Received: 11 May 2007; Revised: 17 July 2008; Accepted: 17 September 2008

ABSTRACT: Currently, calculations of plates in compression are based on the semi-empirical effective width method which was developed by Winter et al.

The effective width method takes the post-buckling capacity into account. The aim of the paper is to establish an effective width method, which is derived on the basis of a consistent theory. The method rests on the theory of plasticity, particularly the yield line theory. Emphasis is on buckling problems related to plate girders. Two general cases are studied: Plates in uniaxial compression supported along all edges, cf. the compressed flange in a box girder, and plates with one free edge, cf. the compressed flange and the transverse web stiffeners in an I-shaped girder.
The results presented coincide closely with Winter's formulae and with tests.

Keywords: Post-buckling, thin plates, theory of plasticity, yield line theory, effective width method, failure mechanisms, stability, in-plane loading

1. INTRODUCTION

It was deduced many years ago that the elastic buckling theory is not able to accurately account for the real strength of plates (Schuman and Back [12]). The main reason for this is that, in a large parameter interval, the ultimate load is reached after yielding of the plate. This fact was also pointed out by Kármán et al. [8], who suggested modifying the elastic solution by an empirical coefficient. This idea was taken up by Winter [15], who developed accurate formulae for the two important cases considered in the following. Winter's method is an *the effective width method*, on which calculations of plates in compression are still based.

Any design method thus has to take into account that plates in compression may carry loads much larger than the load for which elastic buckling will occur.

The aim is here to establish an effective width method, which is derived on the basis of a consistent theory. The method rests on the theory of plasticity, particularly the yield line theory. The new constribution of the paper lies in the way the yield line theory is applied on the deflected shape of the plate. The emphasis is attached to buckling problems related to plate girders. Two general cases are studied: Plates in uniaxial compression supported along all edges, cf. the compressed flange in a box girder, and plates with one free edge, cf. the compressed flange and the transverse web stiffeners in an I-shaped girder.

The basics of the theory are described in Chapter 2. How to take geometrical second order effects into account is illustrated by a column example.

Solutions for plates in uniaxial compression supported along all edges are presented in Chapter 3, while solutions for plates with one free edge are treated in Chapter 4. Both chapters contain a comparison between the theory and the experimental results, on which Winter's formulae were based.

The effect of imperfections is touched upon in Chapter 5 and other possible applications of the theory are mentioned in Chapter 6.

1.1 Historical Overview

Bryan [2] was the first to develop a solution for the elastic critical stress of a rectangular plate simply supported along all edges and subjected to a uniform longitudinal compressive stress. Later a large number of solutions using Bryan's equation have been derived, see for instance (Timoshenko and Gere [14]).

In general the elastic critical stress may be expressed as

$$\sigma_{cr} = k \frac{\pi^2 E}{12\left(1-\nu^2\right)}\left(\frac{t}{b}\right)^2 \tag{1}$$

in which E is Young's modulus, ν Poisson's ratio, t/b the thickness-to-width ratio and k is a buckling coefficient, which is a function of plate geometry and boundary conditions. Useful information on k-factors may be found in a number of references, e.g. (Timoshenko and Gere [14]).

Tests by Schuman and Back [12] on plates supported by V-grooves along the unloaded edges demonstrated that, for plates of the same thickness, an enhancement of the plate width beyond a certain value did not increase the ultimate load. Wider plates acted as though narrow side portions or "effective load-carrying areas" took most of the load. Furthermore, the ultimate load was found to be up to thirty times larger than the elastic critical buckling load determined by Bryan's equation, cf. Eq. 1.

It is now well known that the post-buckling resistance of plates is due to redistribution of axial compressive stresses, and to a lesser extent, to tensile membrane effects and to shear that accompany the out-of-plane bending of the plate in both longitudinal and transverse directions. The longitudinal stresses tend to concentrate in the vicinity of the longitudinally supported edges, which are the stiffer parts of the buckled plate. As a result, yielding begins along these edges, which limits the load-carrying capacity.

Several researchers have been prompted by the tests of Schuman and Back [12] to develop expressions for the ultimate strength of such plates. The first to use the effective width concept in handling this problem was Kármán et al. [8]. They derived the following approximate formula for the effective width, b_e, of plates supported along all edges, based on the assumption that two strips with total width, b_e, along the sides, each on the verge of buckling, carry the entire load:

$$b_e = \frac{\pi}{\sqrt{3\left(1-\nu^2\right)}} t \sqrt{\frac{E}{\sigma_e}} \tag{2}$$

Here σ_e is the edge stress along b_e and the remaining notation is as in Eq. 1.

As a result of many tests and studies of post-buckling strength, Winter [15] suggested the following formula for the effective width:

$$b_e = 1.9t \sqrt{\frac{E}{\sigma_e}}\left(1.0 - 0.574 \frac{t}{b}\sqrt{\frac{E}{\sigma_e}}\right) \tag{3}$$

This equation has been modified several times over the past. In the latest version, adopted in Eurocode for steel structures, EC3 [4], the formula is written as

$$\frac{b_e}{b} = \sqrt{\frac{\sigma_{cr}}{\sigma_e}}\left(1.0 - 0.22\sqrt{\frac{\sigma_{cr}}{\sigma_e}}\right) \tag{4}$$

In the calculation of the ultimate compression load, the edge stress, σ_e, is taken to be equal to the yield stress of the plate material. The elastic critical stress, σ_{cr}, is determined by Eq. 1. Eq. 4 corresponds to Eq. 3 if the factor 0.574 is substituted with a factor of 0.415.

For plates supported along only one longitudinal edge, the effective width has been experimentally determined by Winter [15]. The original formula was

$$b_e = 1.25t\sqrt{\frac{E}{\sigma_e}}\left(1.0 - 0.333\frac{t}{b}\sqrt{\frac{E}{\sigma_e}}\right) \tag{5}$$

This equation has also been modified several times. In the latest version, adopted in EC3 [4], it is written as

$$\frac{b_e}{b} = \sqrt{\frac{\sigma_{cr}}{\sigma_e}}\left(1.0 - 0.188\sqrt{\frac{\sigma_{cr}}{\sigma_e}}\right) \tag{6}$$

In the 1993-edition of EC3 [3], Eq. 4 referred to the case of plates supported along all edges and plates with one free edge. Hence, the difference between the two cases is only the value of the buckling coefficient, *k*. It is practical and convenient to have only one expression. The reason for changing the factor 0.22 to 0.188, for plates with one free edge, is as yet not know to the authors. But the adjustment seems to be rather insignificant.

2. POST-BUCKLING THEORY FOR PLATES IN COMPRESSION

The basic idea is to use plastic theory in the form of limit analysis on the deflected shape of the plate. The deflected shape has to be estimated which is done by using simple formulae from beam and plate theory. The plastic analysis is carried out using yield line theory. Hence, strain hardening is not taken into consideration. Furthermore, the effect of residual stresses is not considered since, according to the theory of plasticity, they have no influence on the load-carrying capacity. Imperfections may easily be taken into account if it is assumed that the imperfections have the same form as the deflected shape of the plate at maximum load.

The contribution of the paper lies in the way the yield line theory is applied on the deflected shape of the plate. Since the deflected shape has to be estimated, the application of the method requires qualified engineering judgement.

2.1 Yield Line Theory

Yield line theory is an upper-bound method. The mechanisms considered are a system of bending yield hinges along lines, *the yield lines*. The load-carrying capacity is determined by the work equation, equalising external work and dissipation in the yield lines.

It is assumed that the plane stress field existing before buckling is known so that the principal normal forces may be found whereby the corresponding yield moments may be determined. In an unloaded direction, the bending capacity, m, reaches the full yield moment per unit length in bending, m_p:

$$m = m_p = \frac{1}{4} t^2 f_y \tag{7}$$

where t is the thickness of the plate and f_y the yield stress. In the direction of a principal compression or tension (normal force n per unit length), the bending capacity, m, is reduced due to the normal force as for beams subjected to combined bending and normal force, i.e.

$$m = m_p \left(1 - \left(\frac{n}{n_p} \right)^2 \right) \tag{8}$$

where m_p is given by Eq. 7 and $n_p = t f_y$ is the load-carrying capacity in pure compression or tension. By determining the yield moments in the two principal directions in this way, the simplification suggested by Johansen [6] may be used to calculate the bending moment in a yield line, m_b, as

$$m_b = m_{px} \sin^2 \beta + m_{py} \cos^2 \beta \tag{9}$$

where β is the angle between the yield line and the x-axis. The x- and y-axes are directed along the principal directions, and m_{px} and m_{py} are the corresponding yield moments per unit length. The plastic yield moments, m_{px} and m_{py}, are determined by either Eq. 7 or Eq. 8. Eq. 9 is correct for reinforced concrete slabs in general, which was shown by Nielsen [11]. It is also correct if the yield condition in principal moment space is square or rectangular. For steel plates, such assumptions are dubious, when the slab is acted upon by torsion. Nevertheless, Eq. 9 is used in the following with surprisingly good results.

A number of different researchers have developed formulae for the plastic moment capacity of inclined yield lines, the first being Murray [10]. Hiriyur and Schafer [5] and Zhao [16] have shown that the solutions obtained by the different proposals vary widely, and Zhao [16] concludes that nothing better than the method suggested by Murray [10] has been found. The present paper aims at improving this state of affairs.

2.2 Effect of Deflections

From the general theory of beam-columns, it is known that the equilibrium equations may be derived for the undeformed structure if a fictitious load is included. The fictitious load is a moment per unit length of the beam, equal to

$$m = N \frac{du}{dx} \tag{10}$$

where N is normal force and u the deflection, transverse to the beam axis, x. The statical equivalence of m may be expressed in several ways, but for a given part of a beam subjected to a constant normal force, N, it may conveniently be expressed in the following simple way: The total moment, M, on a beam (A-B), when N is constant, is

$$M = \int_A^B m\,dx = \int_A^B N\frac{du}{dx}dx = N\int_A^B \frac{du}{dx}dx = N\left(u_B - u_A\right) = N\,\Delta u \tag{11}$$

which may be split into two forces, $N\,\Delta u/L$, in the two end points. The two forces are transverse to the beam as shown in Figure 1.

The value of these forces is independent of the deflected shape between the end points (A and B). Only the difference in the deflection at the end points is important. The work in a virtual displacement, where the beam considered moves as a rigid body, may then be determined as the work done by the two forces, $N\,\Delta u/L$.

In the simple cases considered in the present paper, the above result may be used by considering the plate as being subdivided into strips with constant normal force. In Figure 2, a simply supported square plate subjected to uniaxial compression is shown.

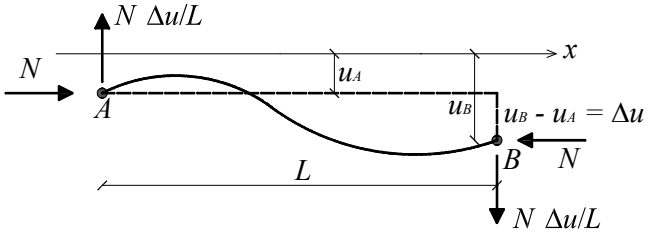

Figure 1. Part of a Beam Subjected to a Constant Normal Force, N, and Statically Equivalent Transverse Forces in the End Points

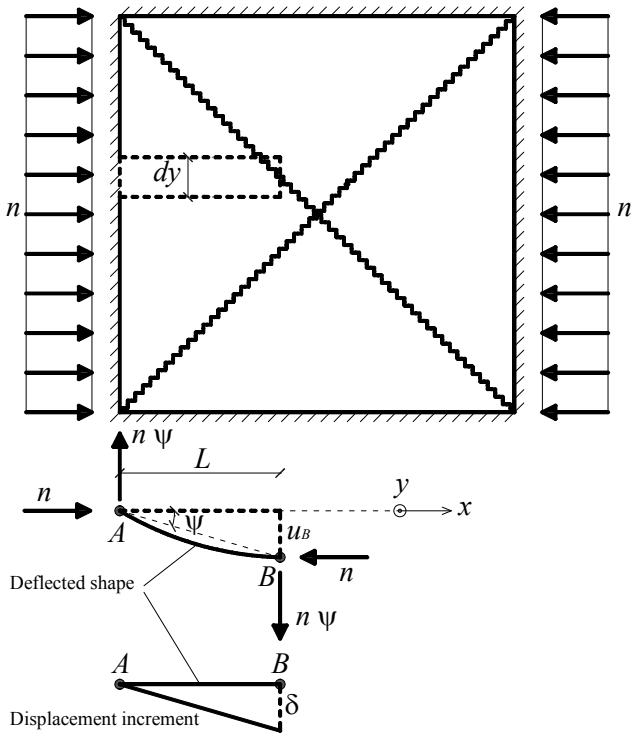

Figure 2. Plate Subdivided into Strips with Infinitesimal Widths

The strip, marked by the dashed lines, has a normal force, n, per unit length. The transverse forces are a uniform load, $n\psi$, along the lines (A and B) acting upwards in (A) (i.e. perpendicular to the x,y-plane), and a uniform load acting downwards in (B). For a displacement increment, δ, along the line (B), the external work for the strip, d_y, is given by

$$dW_e = n\,\psi\,dy\,\delta \tag{12}$$

where the angular deflection increment, $\psi = u_B/L$. The dissipation contribution from the strip is determined by

$$dW_i = m\,dy\,\frac{\delta}{L} \tag{13}$$

where m is calculated by Eq. 8.

2.3 Column Example

The procedure is illustrated by a simply supported column, see Figure 3. The deflected shape of the column is characterised by the deflection in the midpoint at maximum load, u_m. The column is centrally loaded by a compressive normal force, N, and thereby each half is subjected to the forces, $N\psi$. In the figure they are only shown in the midpoint.

The column is given a lateral displacement increment, δ, at the midpoint, as shown in Figure 4, where a plastic yield hinge is formed.

The external work of the mechanism is

$$W_e = 2\,N\,\psi\,\delta = 4\,N\,\frac{u_m}{L}\,\delta \tag{14}$$

and the dissipation is

$$W_i = 4\,\frac{M_p}{L}\,\delta \tag{15}$$

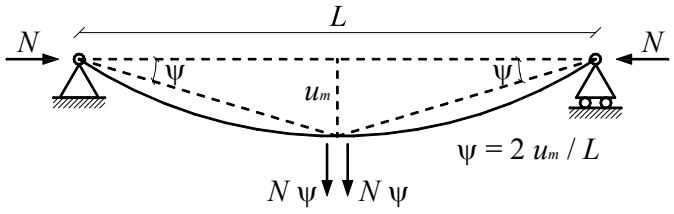

Figure 3. Deflected Shape of a Simply Supported Column

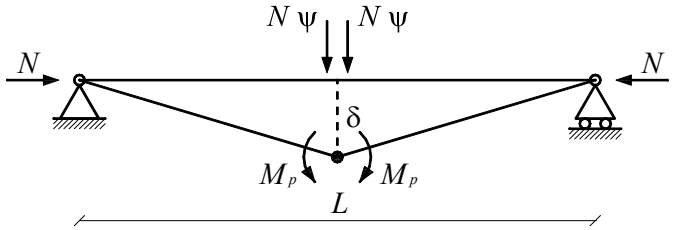

Figure 4. Failure Mechanism for a Lateral Displacement Increment, δ

Here, M_p is the plastic yield moment, which must be reduced due to the normal force.

The work equation renders:

$$N u_m = M_p \tag{16}$$

In this case just, the usual equilibrium equation is found.

A constant, solid and rectangular cross-section of the column is assumed in order to compare the result with the solutions derived later for plates. Hence, the following solution also corresponds to a rectangular plate with two free unloaded edges. The sides of the rectangular cross-section are denoted b and t, respectively, where $b \geq t$ is assumed. The plastic yield moment, reduced due to the normal force, is then

$$M_p = \frac{1}{4} b t^2 f_y \left(1 - \left(\frac{N}{N_p} \right)^2 \right) \tag{17}$$

N is the normal force, f_y the yield stress and $N_p = b\ t\ f_y$ is the load-carrying capacity in pure compression or tension.

The next step is to find a good estimate for the deflected shape of the column. The maximum deflection for a beam may in general be determined as

$$u_m = \frac{1}{\alpha} \kappa L^2 \tag{18}$$

where κ is the curvature in a selected point, L the length and α is a parameter depending on the shape of the curvature function. In the following, $\alpha = 8$, corresponding to a constant curvature function, is used.

In a beam or column with yielding, the deflection corresponding to maximum load tends to be reached when the yield strain, ε_y, is obtained in one or both faces. Here it is assumed that the deflection at maximum load may be found by assuming that the yield strain, $\varepsilon_y = f_y/E$ (f_y is yield stress and E Young's modulus), is reached in both faces. Thus the curvature is determined by $2\ \varepsilon_y / t$. The resulting formula is modified by a parameter, μ, in the following way:

$$\kappa = \frac{2 \varepsilon_y \mu}{t} \tag{19}$$

The parameter, μ, is an empirical coefficient accounting for the effect of imperfections and residual stresses. Hence for the column in Figure 3, the deflection equals:

$$u_m = \frac{1}{8} \frac{2 \varepsilon_y \mu}{t} L^2 = \frac{1}{4} \mu \frac{f_y}{E} \frac{L^2}{t} \tag{20}$$

Inserting Eq. 17 and Eq. 20 into Eq. 16, the load-carrying capacity expressed by the non-dimensional value, $N / (b\ t\ f_y)$, is found to be

$$\frac{N}{b t f_y} = -\frac{1}{2}\mu\lambda^2 + \sqrt{\frac{1}{4}\mu^2\lambda^4 + 1} \tag{21}$$

where the parameter, λ, has been introduced:

$$\lambda = \frac{L}{t}\sqrt{\frac{f_y}{E}} \tag{22}$$

Now this result is compared with the EC3 [4] formulae. Here a non-dimensional slenderness ratio, λ_r, given by

$$\lambda_r = \sqrt{\frac{A f_y}{N_{cr}}} \tag{23}$$

is introduced.

In this formula, A is the cross-sectional area and N_{cr} is the elastic critical buckling force (the Euler-load), see the following Eq. 27. For a solid, rectangular cross-section where λ is given by Eq. 22, λ_r may be expressed as,

$$\lambda_r = \frac{\sqrt{12}}{\pi}\sqrt{\frac{f_y}{E}}\frac{L}{t} = \frac{\sqrt{12}}{\pi}\lambda \tag{24}$$

The load-carrying capacity according to EC3 [4] is given by

$$\frac{N_{cr}}{b t f_y} = \frac{1}{\Phi + \sqrt{\Phi^2 - \lambda_r^2}} \tag{25}$$

where

$$\Phi = 0.5\left(1 + \alpha\left(\lambda_r - 0.2\right) + \lambda_r^2\right) \tag{26}$$

The so-called *geometric equivalent imperfection factor* α in this equation may be obtained from Table 1. Notice that α here is not the same as the α introduced in Eq. 18.

The buckling curves according to EC3 [4], cf. Eq. 25, and the curve given by Eq. 21 for $\mu = 1.4$ are shown in Figure 5. It turns out that by choosing a value of μ between 1.2 and 1.6, all buckling curves in EC3 [4] may be well represented. For $\mu = 1.4$, the result coincides very closely with the buckling curve *b*. The figure also shows the Euler curve, which for a solid rectangular cross-section is given by

$$\frac{N_{cr}}{b t f_y} = \frac{1}{\lambda_r^2} = \frac{\pi^2}{12}\lambda^{-2} \tag{27}$$

Table 1. Imperfection Factors for Buckling Curves According to EC3

Buckling curve	a_0	*a*	*b*	*c*	*d*
Imperfection factor α	0.13	0.21	0.34	0.49	0.76

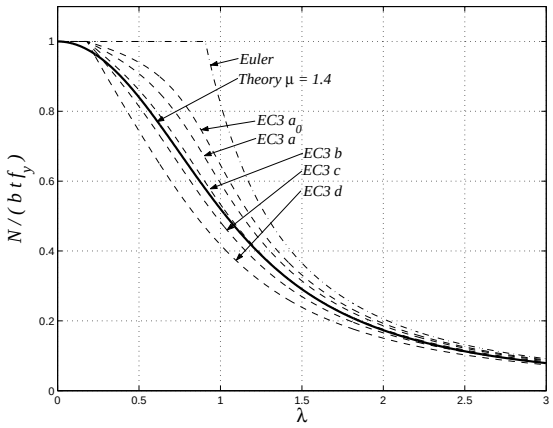

Figure 5. $N / (b\, t\, f_y)$ as a Function λ, Plastic Theory and EC3

If the column in Figure 3 is also subjected to a lateral load, q, per unit length along the entire length, L, then this load is easily included in the calculations. The work done by the lateral load is simply added to the external work, thus the work equation becomes, cf. Eq. 16,

$$N u_m + \frac{1}{8} q L^2 = M_p \tag{28}$$

Other column cases may be treated in a similar way but this is not our purpose here.

3 PLATES SUPPORTED ALONG ALL EDGES

The compression flange in a box-girder may be considered as a plate simply supported along all edges. How to determine the post-buckling strength of plates supported along all edges is presented below.

3.1 Square Plates

The square plate in Figure 6 is considered. It is simply supported along all four edges and subjected to a uniform load per unit length, n, along two opposite edges.

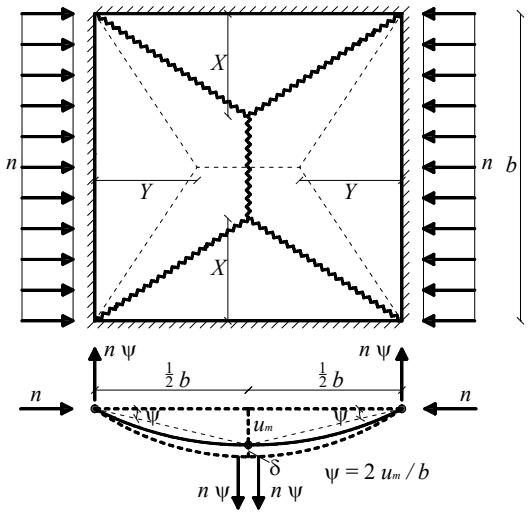

Figure 6. Failure Mechanism for a Simply Supported Square Plate

The first step is to find a good estimate for the deflected shape of the plate. As stated in Section 2.3, the maximum deflection for a beam may in general be determined as

$$u_m = \frac{1}{\alpha}\kappa L^2 \tag{29}$$

where κ is the curvature, L the length and α is a parameter depending on the shape of the curvature function. In the following $\alpha = 8$ is used, corresponding to a constant curvature function.

In a plate with yielding, the deflection corresponding to maximum load, as mentioned above, tends to be reached when the yield strain, ε_y, is obtained in one or both faces. As in the case of a column, cf. Section 2.3, the deflection at maximum load may be found by assuming that the yield strain, $\varepsilon_y = f_y/E$, is reached in both faces of the plate. Here, f_y is the yield stress and E is the Young's modulus. In this case $\mu = 1$ is applied, cf. Eq. 19, thus the curvature is determined by (t being the plate thickness)

$$\kappa = \frac{2\varepsilon_y}{t} \tag{30}$$

For a square plate, L is taken equal to the side length, b. Hence, for the plate in Figure 6, the deflection at maximum load, u_m, is

$$u_m = \frac{1}{8}\frac{2\varepsilon_y}{t}b^2 = \frac{1}{4}\frac{f_y}{E}\frac{b^2}{t} \tag{31}$$

The next step is to find the optimal failure mechanism (yield line pattern). In Figure 6, two different yield line patterns are shown, one with the free parameter, X, and one with the free parameter, Y (shown with dashed lines), respectively.

For the mechanism with the free parameter, X, the external work for a displacement increment, δ, equals

$$\begin{aligned} W_e &= 4X n\frac{2u_m}{b}\frac{\delta}{2} + 2(b-2X)n\frac{2u_m}{b}\delta \\ W_e &= n u_m \delta\left(4 - 4\frac{X}{b}\right) \end{aligned} \tag{32}$$

and the dissipation is

$$W_i = 4m_p\,\delta\left(1 - \left(\frac{n}{n_p}\right)^2\right) + 2m_p\,\delta\frac{b}{X} \tag{33}$$

Here, the plastic yield moment, m_p, per unit length is given by Eq. 7 and $n_p = t\,f_y$ is the load-carrying capacity in pure compression or tension.

Equalising the external work and the dissipation and inserting Eq. 7 and Eq. 31, the load-carrying capacity, expressed by the non-dimensional parameter, $n/(t\,f_y)$, may be written as

$$\frac{n}{t f_y} = -\frac{1}{2}\lambda^2\left(1-\frac{X}{b}\right)+\sqrt{\frac{1}{4}\lambda^4\left(1-\frac{X}{b}\right)^2+\frac{1}{2}\left(2+\frac{b}{X}\right)} \tag{34}$$

where the parameter, λ,

$$\lambda = \frac{b}{t}\sqrt{\frac{f_y}{E}} \tag{35}$$

has been introduced.

Eq. 34 is the post-buckling load in this case. The value of $n/(t f_y)$ as a function of λ is shown for different values of X in Figure 7.

It is seen that $n/(t f_y) > 1$ for small values of λ, which is not possible in reality, hence a cut-off at $n/(t f_y) = 1$ must be introduced. With this cut-off, it appears that almost the same load-carrying capacity is obtained for $X = 1/2\ b$, $X = 2/5\ b$ and $X = 1/3\ b$.

The mechanism with the free parameter, Y, cf. Figure 6, leads to $Y = 0$ when optimised. However, it must be remembered that the deflected shape is used both as an estimate of the deflection at maximum load and as the basis for a choice of the deflection increment at the yield load. Thus a normal optimisation may not be appropriate. The optimised value for $Y = 0$ is therefore disregarded and the mechanism corresponding to $X = ½\ b$ ($Y = ½\ b$) is chosen for the following calculations.

In Figure 8, the ratio, $n/(t f_y)$, as a function of λ for $X = 1/2\ b$ is shown together with the elastic solution, which may be written as, cf. Eq. 1,

$$\frac{n}{t f_y} = \frac{\pi^2 k}{12\left(1-\nu^2\right)}\lambda^{-2} \tag{36}$$

where k is the buckling coefficient and ν is Poisson's ratio. Here $k = 4$ and $\nu = 0.30$ are used. The parameter, λ, is given by Eq. 35.

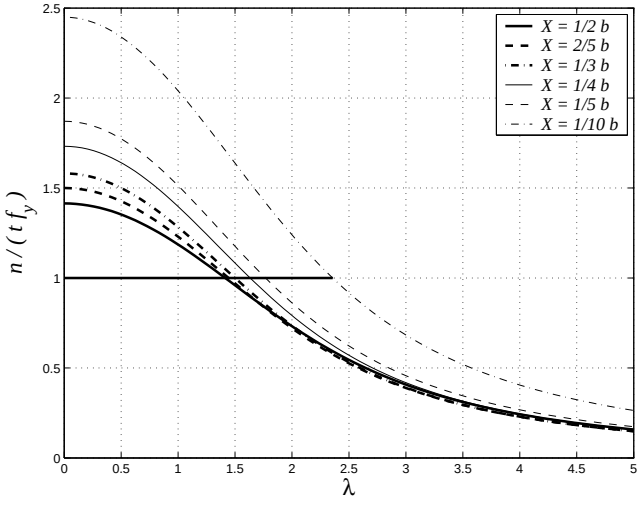

Figure 7. $n/(t f_y)$ as a Function of λ for Different Values of X

The two curves coincide very closely, which would indicate that no extra post-buckling reserve is found from this approach. However, the result is incorrect, which is due to the fact that a redistribution of the stresses occurs when the buckling mechanism develops. This is illustrated in Figure 9.

As previously mentioned, Kármán et al. [8] suggested that the redistribution may be taken into account by using an effective area subjected to a uniform stress equal to the yield stress, i.e. $\sigma = f_y$ in Figure 9. The same simplification will be used here. Hence the considered plate is subjected to a load per unit length equal to the yield stress multiplied by the thickness of the plate, i.e. $n = n_p = tf_y$, which is applied along two strips with the width equal to the unknown width b_s, see Figure 10.

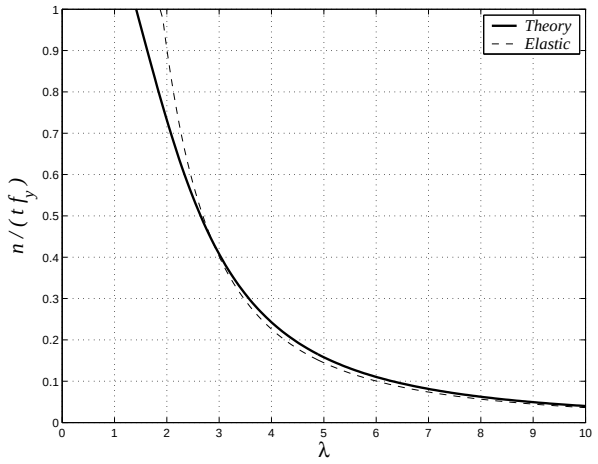

Figure 8. $n/(tf_y)$ as a Function of λ for $X = ½\ b$

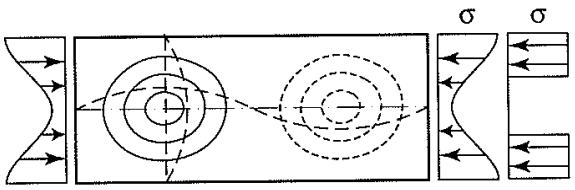

Figure 9. Redistribution of Edge Stresses During Buckling

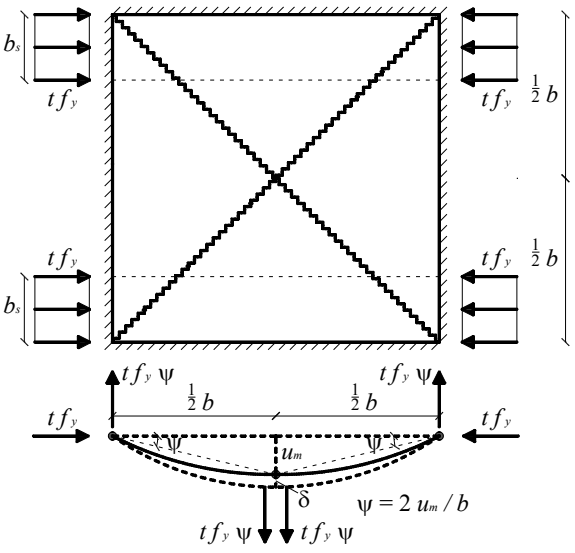

Figure 10. Simply Supported Square Plate Subjected to Uniaxial Compression Along Strips of width b_s

The external work, W_e, and the dissipation, W_i, are for $\delta = 1$, respectively:

$$W_e = 8\,t\,f_y\,u_m\,\frac{b_s^2}{b^2} \tag{37}$$

$$W_i = \underbrace{8\,m_p\,\frac{b_s}{b}\left(1-\left(\frac{t\,f_y}{n_p}\right)^2\right)}_{=0} + 8\,m_p\left(1-\frac{b_s}{b}\right) = 8\,m_p\left(1-\frac{b_s}{b}\right) \tag{38}$$

Again, u_m is the deflection at maximum load, m_p is the plastic yield moment per unit length given by Eq. 7 and $n_p = t\,f_y$ is the load-carrying capacity in pure compression or tension.

The contribution from the part of the yield lines running in the widths, b_s, is equal to zero, as $n_p = t\,f_y$. Inserting Eq. 7 and Eq. 31, and using $W_i = W_e$, b_s is found to be determined by

$$\frac{f_y}{E}b_s^2 + \frac{t^2}{b}b_s - t^2 = 0 \tag{39}$$

Denoting the total effective width $b_e = 2\,b_s$, we find

$$\frac{b_e}{b} = -\lambda^{-2} + \sqrt{\lambda^{-4} + 4\,\lambda^{-2}} \tag{40}$$

where λ is given by Eq. 35.

The average stress relative to the yield stress, f_y, along the whole width, b, from the yield force, $b_e\,t\,f_y$, along b_e is $b_e\,t\,f_y/(b\,t\,f_y) = b_e/b$. For a solution with uniform load, n, along the whole width, b, the average stress relative to the yield stress is $n/(t\,f_y)$.

In Figure 11, b_e/b, cf. Eq. 40, is shown as a function of λ.

The elastic buckling load characterised by $n/(t\,f_y)$, cf. Eq. 36, is also shown. It appears that the plate may carry compressive forces considerably above the elastic buckling load. The first to demonstrate this through tests appear to be Schuman and Back [12].

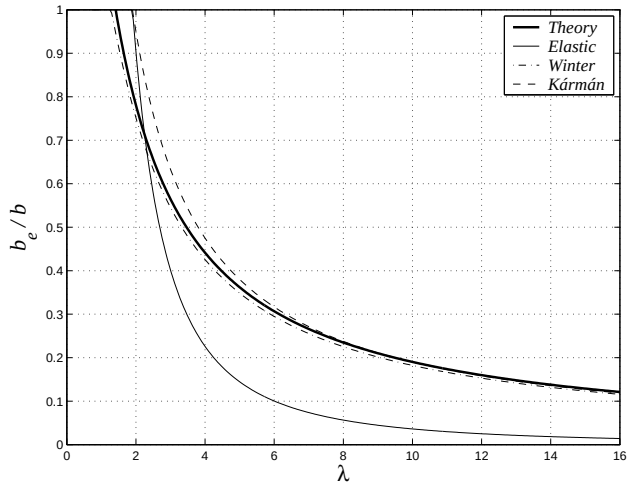

Figure 11. b_e/b as a function of λ

The third curve plotted in the figure is the semi-empirical expression derived by Winter [15]. With the introduced parameter, λ, given by Eq. 35, it may be written as, cf. Eq. 4,

$$\frac{b_e}{b} = \frac{\pi\sqrt{k}}{\sqrt{12\left(1-\nu^2\right)}}\lambda^{-1}\left(1-0.22\frac{\pi\sqrt{k}}{\sqrt{12\left(1-\nu^2\right)}}\lambda^{-1}\right) \tag{41}$$

Finally, a cut-off at $b_e/b = n/(t f_y) = 1$ has been introduced.

Winter's formula is a modification of the original formula introduced by Kármán et al. [8]:

$$\frac{b_e}{b} = C\frac{t}{b}\sqrt{\frac{E}{f_y}} = C\lambda^{-1} \tag{42}$$

where C is an empirical constant. Based on the tests made by Schuman and Back [12], $C = 1.9$ was found. Eq. 42 is also shown in the figure.

Regarding Eq. 42, Winter [15] argued that C should depend on the parameter λ^{-1}. Based on his own tests and those made by Sechler (Winter [15]), he found the best fit to be

$$C = 1.9 - 1.09\frac{t}{b}\sqrt{\frac{E}{f_y}} = 1.9 - 1.09\lambda^{-1} \tag{43}$$

As previously mentioned, this formula has later been modified several times.

Eq. 41 is the newest modification and it is adopted in EC3 [4]. Eq. 41 corresponds, for $k = 4$ and for $\nu = 0.30$, to

$$C = 1.9 - 0.42\lambda^{-1} \tag{44}$$

Figure 11 shows that the present theoretical result closely follows Winter's semi-empirical solution.

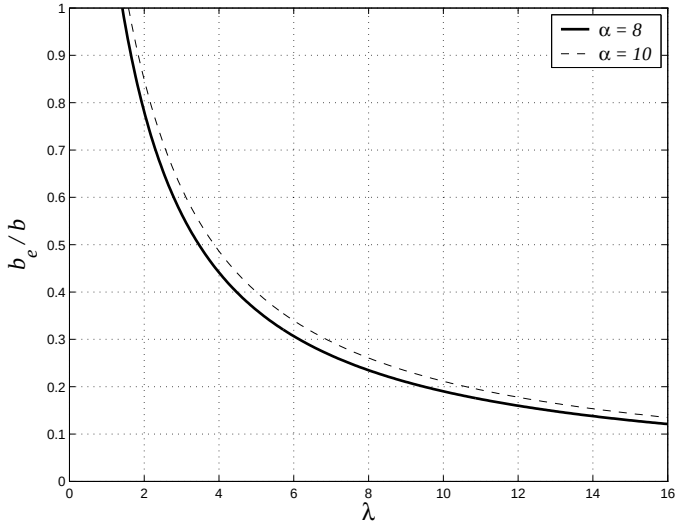

Figure 12. b_e/b as a Function of λ for $\alpha = 8$ and $\alpha = 10$, respectively

In order to investigate the sensitiveness of the solution, Eq. 40, to the estimated deflection at maximum load, it is compared with the solution using $\alpha = 10$ in Figure 12.

Choosing $\alpha = 10$ in Eq. 29 approximately corresponds to a sinusoidal curvature function ($\alpha = \pi^2 \approx 10$). For $\alpha = 10$, the effective width is determined by

$$\frac{b_e}{b} = -\frac{5}{4}\lambda^{-2} + \sqrt{\frac{25}{16}\lambda^{-4} + 5\lambda^{-2}} \tag{45}$$

where λ is still given by Eq. 35.

Eq. 45 gives a post-buckling strength up to 11 % larger than that obtained by Eq. 40 for the λ-interval shown in Figure 12. Hence, the theory seems to be relatively insensitive to the estimated deflection at maximum load.

When von Mises' yield criterion is applied, m_p in Eq. 38 is replaced by $2m_p/\sqrt{3}$ if uniaxial strain is supposed. In that case also n_p should be increased and b_e/b then will measure n relative to the increased value of n_p. Thus it turns out that nothing is changed, since b_e/b is still given by, cf. Eq. 40,

$$\frac{b_e}{b} = -\lambda^{-2} + \sqrt{\lambda^{-4} + 4\lambda^{-2}} \tag{46}$$

In practise one is on the safe side by using the uniaxial yield stress. Thus the former solution is applied.

3.2 Rectangular Plates

It is a well-known fact that a long rectangular elastic plate subjected to compression in the longitudinal direction buckles into a shape of half waves with a length equal to the plate width, see Figure 13. This result is applied when estimating the post-buckling strength. Thus a long plate is subdivided into a number of square plates where the previous yield line patterns may be applied, cf. Section 3.1. The vertical lines between the square regions will act as simple supports, since if one square region forms a wave downwards, then the adjacent regions will form a wave upwards. Therefore, the post-buckling strength or the effective width for a long rectangular plate is in general given by Eq. 40.

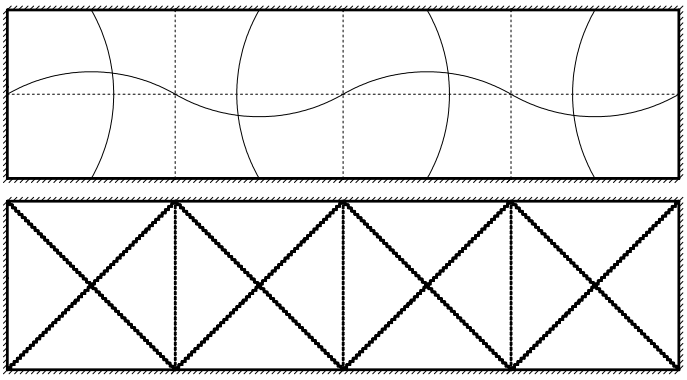

Figure 13. Deflection Shape and Failure Mechanism for Long Simply Supported Rectangular Plates

Now consider a rectangular plate with a length somewhat larger than the width. In Figure 14, the width is named b and the length named a. The plate is subjected to uniaxial compression, $n_p = t f_y$, acting on the two strips, b_s.

The failure mechanism has the free parameter, X. The maximum deflection, u_m, is assumed to be given by Eq. 31. The external work is then for $\delta = 1$ given by

$$W_e = 4 t f_y \frac{u_m}{X} \frac{b_s^2}{b} \tag{47}$$

and the dissipation

$$W_i = 2 m_p \left(\frac{b}{X} - 2\frac{b_s}{X} + 2\frac{a}{b} \right) \tag{48}$$

Hence, b_s may be determined by

$$\frac{f_y}{E} b_s^2 + \frac{t^2}{b} b_s - t^2 \left(\frac{1}{2} + \frac{X a}{b^2} \right) = 0 \tag{49}$$

The effective width, b_e ($b_e = 2\, b_s$), is then found to be

$$\frac{b_e}{b} = -\lambda^{-2} + \sqrt{\lambda^{-4} + 4\left(\frac{1}{2} + \frac{X a}{b^2} \right) \lambda^{-2}} \tag{50}$$

where λ is given by Eq. 35. Furthermore, in the above equations, t is the thickness, E is Young's modulus, f_y the yield stress, m_p is the plastic yield moment per unit length given by Eq. 7, and $n_p = t f_y$ is the load-carrying capacity in pure compression or tension.

Assuming $X = ½\, b$, the effective width is determined by

$$\frac{b_e}{b} = -\lambda^{-2} + \sqrt{\lambda^{-4} + 2\left(1 + \frac{a}{b} \right) \lambda^{-2}} \tag{51}$$

When a is larger than, or equal to, b, it appears that Eq. 51 gives the smallest post-buckling strength if a is equal to b. Hence in practice, the yield line pattern for a square plate may be considered as the optimal solution, rather than the pattern shown in Figure 14.

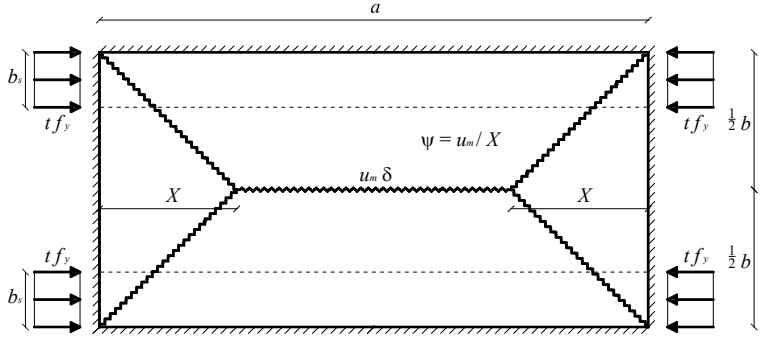

Figure 14. Failure Mechanism for a Short Rectangular Plate

Special attention is required for plates where a is smaller than b, but the theory may also easily be applied to this case.

The yield line pattern shown in Figure 15 is considered, where a is still larger than b but the loaded strips are now vertical. The plate is subjected to a load per unit length equal to the yield stress, f_y, multiplied by the thickness, t, along two strips of width b_s. The failure mechanism has the free parameter, X. The work equation must be derived separately for the two cases, $b_s < X$ and $b_s > X$, respectively.

In the case $b_s < X$, the external work for $\delta = 1$ is given by

$$W_e = 4\,t\,f_y\,\frac{u_m}{b\,X}\,b_s^2 \tag{52}$$

and the dissipation

$$W_i = 4\,m_p\left(\frac{a}{b} - 2\frac{b_s}{b} + \frac{1}{2}\frac{b}{X}\right) \tag{53}$$

where m_p is the plastic yield moment per unit length given by Eq. 7.

The maximum deflection, u_m, is taken as the deflection of a beam in the direction of the uniaxial compression with the curvature given by Eq. 30. Thus

$$u_m = \frac{1}{8}\frac{2\varepsilon_y}{t}b^2 = \frac{1}{4}\frac{f_y}{E}\frac{b^2}{t} \tag{54}$$

Equalising the external work and the dissipation, the width of each strip, b_s, for $b_s < X$ is found to be determined by

$$\frac{f_y}{E}b_s^2 + 2\frac{t^2\,X}{b^2}b_s - t^2\left(\frac{a\,X}{b^2} + \frac{1}{2}\right) = 0 \tag{55}$$

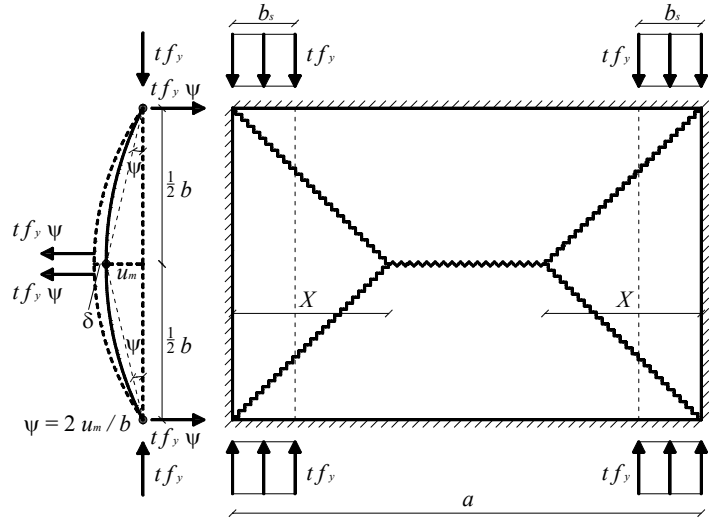

Figure 15. Failure Mechanism for a Web Plate with $a > b$ and $b_s < X$

In the case $b_s > X$, the external work for $\delta = 1$ is given by

$$W_e = 4\,t\,f_y\,\frac{u_m}{b}\left(2\,b_s - X\right) \tag{56}$$

and the dissipation, which is identical to Eq. 53, is

$$W_i = 4\,m_p\left(\frac{a}{b} - 2\frac{b_s}{b} + \frac{1}{2}\frac{b}{X}\right) \tag{57}$$

Equalising the external work and the dissipation, the width of each strip, b_s, for $b_s > X$ is found to be determined by

$$\left(2\frac{f_y}{E}b + 2\frac{t^2}{b}\right)b_s = \frac{f_y}{E}b\,X + t^2\left(\frac{a}{b} + \frac{1}{2}\frac{b}{X}\right) \tag{58}$$

In Section 3.1, it was shown that inclined yield lines under an angle of 45° are normally a good choice, noting that minimising b_s with regard to X did not lead to any useful result. Hence, an angle of 45° is also chosen here, i.e. $X = ½\,b$.

Denoting the effective width $b_e = 2\,b_s$, the effective width for $b_s < X$ ($\Rightarrow b_e < b$) is given by

$$\frac{b_e}{a} = -\lambda^{-2}\frac{b}{a} + \sqrt{\lambda^{-4}\left(\frac{b}{a}\right)^2 + 2\lambda^{-2}\left(\frac{b^2}{a^2} + \frac{b}{a}\right)} \tag{59}$$

and for $b_s > X$ ($\Rightarrow b_e > b$)

$$\frac{b_e}{a} = \frac{\frac{1}{2}\lambda^2\frac{b}{a} + \frac{b}{a} + 1}{\lambda^2 + 1} \tag{60}$$

In both Eq. 59 and Eq. 60, $b_e/b \le 1$ is required, and λ is given by Eq. 35.

The parameter, b_e/a, through Eq. 59 and Eq. 60 as a function of λ is shown for different values of a/b in Figure 16. In Figure 17, the ratio, b_e/b, as a function of λ is shown for different values of a/b. For the two cases treated above, the ratio, b_e/b, may be written as:

For $b_e/b \le 1$:

$$\frac{b_e}{b} = -\lambda^{-2} + \sqrt{\lambda^{-4} + 2\lambda^{-2}\left(\frac{a}{b} + 1\right)} \tag{61}$$

For $b_e/b \ge 1$:

$$\frac{b_e}{b} = \frac{\frac{1}{2}\lambda^2 + \frac{a}{b} + 1}{\lambda^2 + 1} \tag{62}$$

By inserting $b_e/b = 1$ in either Eq. 61 or Eq. 62, it is found that the two curves, for any value of a/b, in both Figure 16 and Figure 17, intersect for

$$\lambda = \sqrt{2\frac{a}{b}} \tag{63}$$

Since, $b_e \leq a$ is required, a cut-off at $b_e/a = 1$, as shown in Figure 16, must be done for all curves. In Figure 17, it is shown that each curve has a cut-off for b_e/b equal to the value of a/b corresponding to the actual curve. By inserting $b_e = a$ into, for instance, Eq. 62, it is verified that the cut-off, in both Figure 16 and Figure 17, takes place for

$$\lambda = \left(\frac{a}{b} - \frac{1}{2}\right)^{-1/2} \tag{64}$$

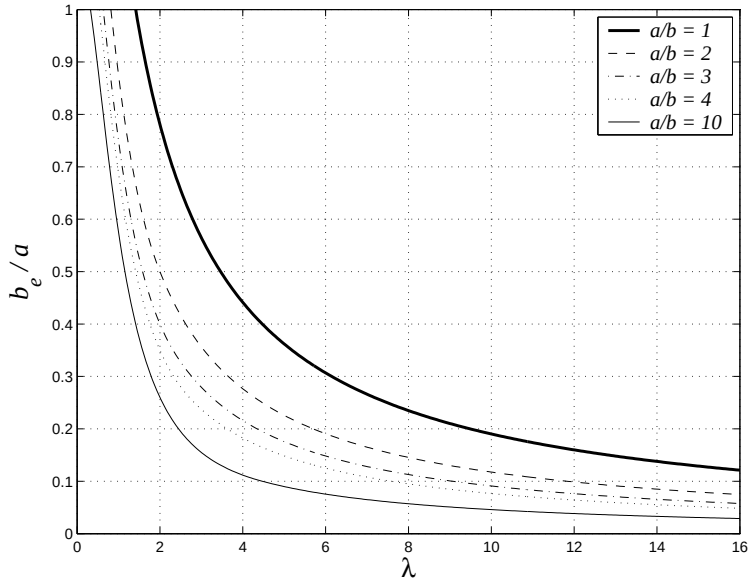

Figure 16. b_e/a as a Function of λ for Different Values of a/b

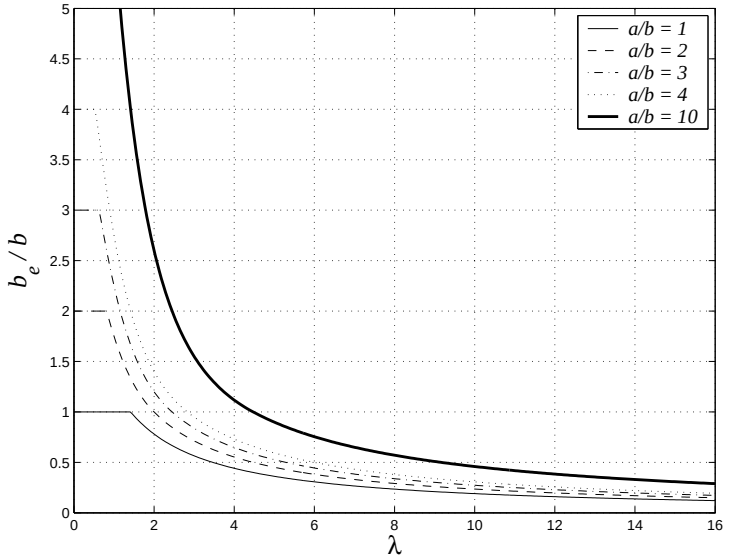

Figure 17. b_e/b as a Function of λ for Different Values of a/b

3.3 Comparison with Experimental Results

The Schuman and Back [12] tests dealt with separate rectangular flat plates of four different metals, i.e. *Duralumin*, *Stainless Iron*, *Monel Metal* and *Nickel*. Eq. 40 is compared to these tests in Figure 18. The figure also shows the elastic solution, cf. Eq. 36, Winter's solution cf. Eq. 41 and the solution by Kármán et al. cf. Eq. 42. From the figure it appears that all formulae, except the elastic solution, overestimate the post-buckling strength, in some cases considerably. However, it is generally accepted that these experiments are unreliable because of the dubious V-groove supports. Hence, these experiments are not treated further here.

In Figure 19, the theories are compared with more reliable experiments.

The *U-beams* and *I-beams* tests made by Winter [15] both consisted of specimens made by bolting or welding U-sections together. Winter also used the tests made by *Sechler* (Winter [15]) to verify his method. The specimens in these tests were single plates, unconnected to any adjacent elements. These tests have been shown in Figure 19. Furthermore, newer tests by Moxham [9] are included in the figure. He conducted three test series, denoted *Welded*, *Unwelded* and *Short* in the following. Also, in these tests, all specimens were separate plates. He developed a new test rig, where he could establish the simple support conditions in a reliable way. In the *Welded* series, the longitudinal edges were heat treated in order to induce residual stresses. The *Short* series was conducted on specimens where the loaded edges were slightly longer than the unloaded edges (length-to-width ratio: 0.875). The theoretical effective width of the short specimens is calculated by Eq. 59 and Eq. 60. The specimens in the *Welded* and *Unwelded* series all had a length-to-width ratio of 4.0.

The agreement with all the tests seems to be very good. In Figure 20, the correlation between the present theory and tests is shown in a more illustrative way. For all tests, a mean value of 1.088 and a standard deviation of 16.9 % are obtained. For the separate test series, the following results are obtained:

- *Sechler*: Mean 1.202, standard deviation 17.9 %.
- Winter, *U-beams*: Mean 1.098, standard deviation 18.9 %.
- Winter, *I-beams*: Mean 1.019, standard deviation 4.6 %.
- Moxham, *Welded*: Mean 1.097, standard deviation 12.2 %.
- Moxham, *Unwelded*: Mean 0.931, standard deviation 5.8 %.
- Moxham, *Short*: Mean 0.946, standard deviation 6.4 %.

It may be seen that the tests by *Sechler* deviate somewhat from the theory, especially for b_e/b close to unity. One explanation for this might be initial imperfections, see Chapter 5. Moreover, he may have applied the same doubtful V-groove supports as Schuman and Back [12]. Without Sechler's tests, a mean value of 1.045 and a standard deviation of 14.4 % are obtained.

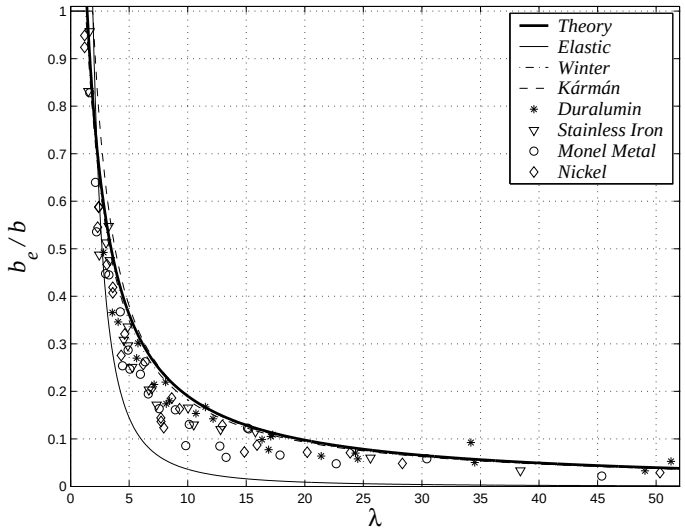

Figure 18. b_e/b as a Function of λ, Theories Compared with Tests by Schuman and Back

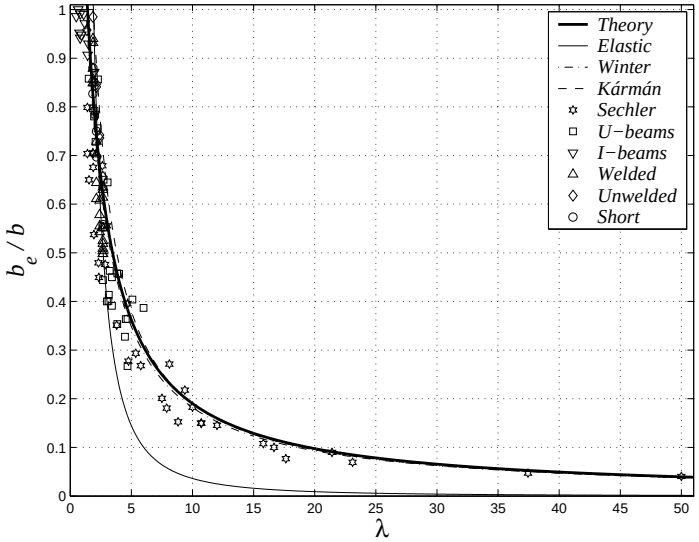

Figure 19. b_e/b as a Function of λ, Theories and Tests

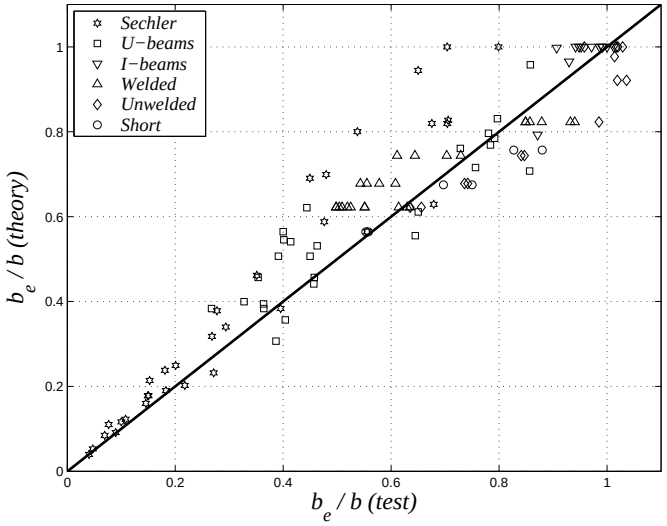

Figure 20. Theory Versus Tests

4. PLATES WITH ONE FREE EDGE

The compressive flange and the transverse web stiffeners in an I-shaped steel plate girder may be considered to be long, rectangular plates simply supported along three of the edges, and free along one longitudinal edge. How to determine the post-buckling strength of such plates is presented below.

4.1 Rectangular Plates

The considered plate with length a, width b and thickness t is subjected to uniaxial compression, $n_p = t f_y$, along an effective width, b_e, near the supported longitudinal edge.

The best failure mechanism, with free parameter, X, is shown in Figure 21. It is easily verifiable that plates with length, a, in the interval, $2X \le a \le \infty$, will have the same post-buckling strength. Plates with $a < 2X$ require another failure mechanism, which will be treated in Section 4.3.

The two regions with area, $X b$, will approximately be subjected to pure torsion. Thus the principal directions are under 45° with the edges, and the principal curvatures are equal, but with opposite sign. In the principal directions, the curvatures are estimated to be, in absolute value, the same as in Eq. 30. Then the torsional curvature, κ_{xy}, will also be $\kappa_{xy} = 2\,\varepsilon_y / t$ ($\varepsilon_y = f_y/E$ is the yield strain and t the thickness), which means that the deflection, u_m, at the end point of the yield line in the free edge will be

$$u_m = \kappa_{xy} X b = \frac{2\varepsilon_y}{t} X b = 2\frac{f_y}{E}\frac{X b}{t} \tag{65}$$

For the mechanism shown in Figure 21, the external work is for $\delta = 1$ given by

$$W_e = t f_y \frac{u_m}{X}\frac{b_e^2}{b} \tag{66}$$

and the dissipation is

$$W_i = 2 m_p \left(\frac{X}{b} + \frac{b}{X} - \frac{b_e}{X} \right) \tag{67}$$

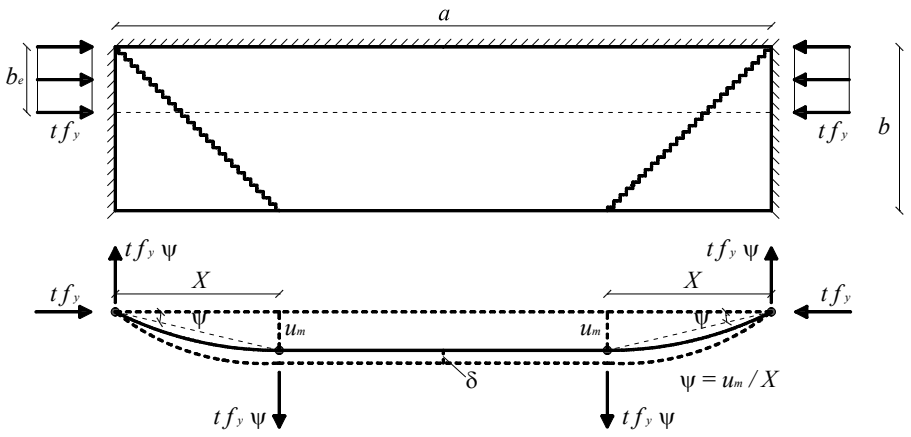

Figure 21. Failure Mechanism for a Rectangular Plate with One Free Edge

where m_p is given by Eq. 7. Hence the effective width, b_e, may be determined by

$$2\frac{f_y}{E}b_e^2+\frac{1}{2}\frac{t^2}{X}b_e-\frac{1}{2}t^2\left(\frac{X}{b}+\frac{b}{X}\right)=0 \tag{68}$$

The non-dimensional value, b_e/b, is then given by

$$\frac{b_e}{b}=-\frac{1}{8}\frac{b}{X}\lambda^{-2}+\sqrt{\frac{1}{64}\left(\frac{b}{X}\right)^2\lambda^{-4}+\frac{1}{4}\left(\frac{X}{b}+\frac{b}{X}\right)\lambda^{-2}} \tag{69}$$

Eq. 69 is shown for different values of X in Figure 22. A cut-off at $b_e/b = 1$ must again be introduced. With this cut-off, it is seen that almost the same load-carrying capacity is obtained for $X = b$, $X = 4/5\ b$ and $X = 3/4\ b$; hence $X = b$ is used in the following calculations.

The effective width for X equal to b is found to be

$$\frac{b_e}{b}=-\frac{1}{8}\lambda^{-2}+\sqrt{\frac{1}{64}\lambda^{-4}+\frac{1}{2}\lambda^{-2}} \tag{70}$$

which is shown in Figure 23. The figure also shows the elastic buckling curve given by Eq. 36 with $k = 0.43$, cf. (Timoshenko and Gere [14]). Again, Poisson's ratio $\nu = 0.30$ is assumed. The third curve shown is Winter's formula in the form given in EC3 [4], which may be written as, cf. Eq. 6,

$$\frac{b_e}{b}=\frac{\pi\sqrt{k}}{\sqrt{12\left(1-\nu^2\right)}}\lambda^{-1}\left(1-0.188\frac{\pi\sqrt{k}}{\sqrt{12\left(1-\nu^2\right)}}\lambda^{-1}\right) \tag{71}$$

Here, $k = 0.43$ and $\nu = 0.30$ are again used. It is found that the theory gives a slightly larger post-buckling strength than Winter's solution.

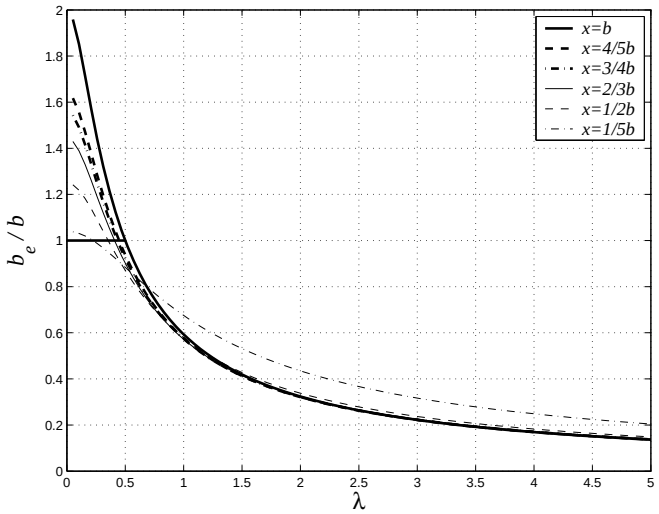

Figure 22. b_e/b as a Function of λ for Different Values of X

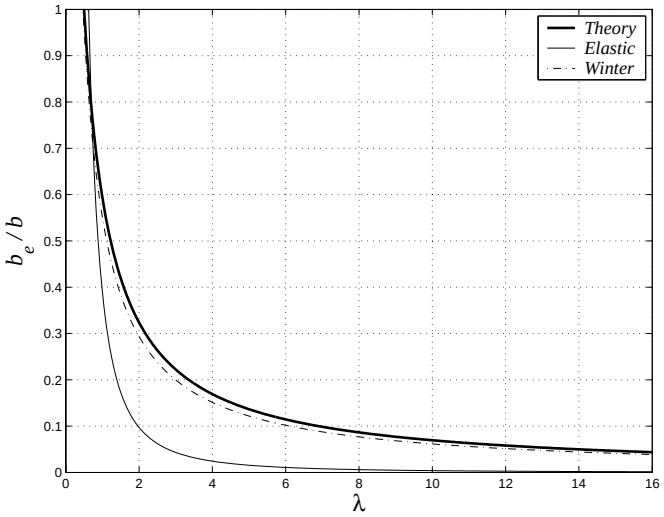

Figure 23. b_e/b as a Function of λ

4.2 Comparison with Experimental Results

Figure 24 shows four test series compared with Eq. 70. The figure also shows the elastic solution cf. Eq. 36 and Winter's solution cf. Eq. 71.

In the test series *Plates* (Bambach and Rasmussen [1]), the specimens were single plates, unconnected to any adjacent elements. These authors applied the test rig suggested by Moxham [9] which enabled them to establish simple support conditions in a reliable way. The series *Stub-column*, *Beams* (Kalyanaraman et al. [7]) and *I-beams* (Winter [15]) all consisted of specimens made by bolting or welding U-sections together.

In Figure 25, the correlation between theory and test is shown. For all tests, a mean value of 0.877 and a standard deviation of 15.7 % are obtained. For the separate test series, the following results are obtained:

- Bambach & Rasmussen, *Plates*: Mean 0.981, standard deviation 8.5 %.
- Kalyanaraman et al., *Stub-column*: Mean 0.717, standard deviation 6.2 %.
- Kalyanaraman et al., *Beams*: Mean 0.790, standard deviation 12.1 %.
- Winter, *I-beams*: Mean 0.925, standard deviation 16.7 %.

The theory seems to underestimate the post-buckling strength for the tests *Stub-column* and *Beams*. Kalyanaraman et al. [7]) stated that the mean value of the elastic buckling coefficient was measured to be around $k = 0.85$. This number shows that the longitudinal edges cannot have been simply supported, since for a plate with a simply supported longitudinal edge $k = 0.43$. For a fixed edge $k = 1.28$ according to the elastic theory, cf. (Timoshenko & Gere [14]). The test series *I-beams* is defected by a large scatter. Winter [15] gives several explanations for the large scatter. On the other hand, the test series *Plates*, with the most reliably established boundary conditions, shows a very good agreement with the theory.

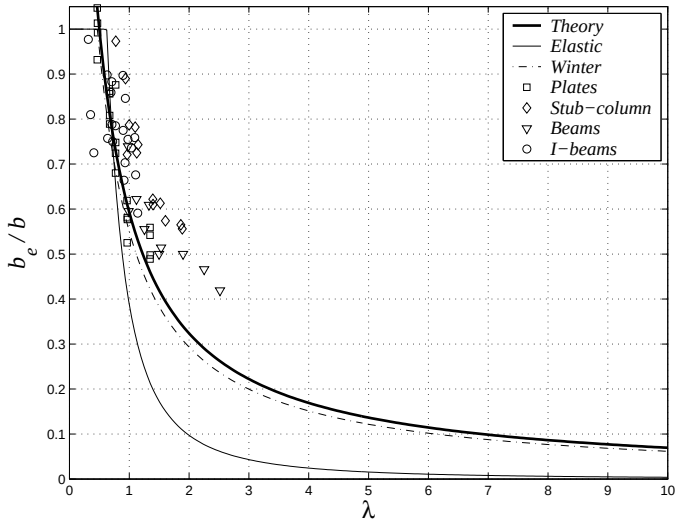

Figure 24. b_e/b as a Function of λ, Theories and Tests

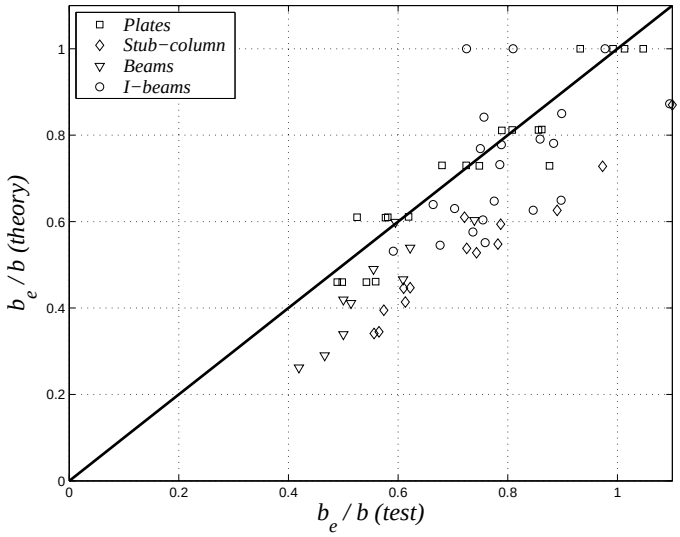

Figure 25. Theory Versus Tests

4.3 Square Plates

Square plates in uniaxial compression with one free edge require another failure mechanism than the one shown in Figure 21 valid for rectangular plates.

The optimal mechanism for a square plate is drawn in Figure 26. It has the free parameter, X, which is set at $X = ½\ b$. The plate is again subjected to uniaxial compression, $n_p = t\, f_y$, along an effective width, b_e, close to the support.

In this case, two work equations must be derived; one corresponding to $b_e < X$ and one corresponding to $b_e > X$, respectively.

The deflection at maximum load, u_m, is taken as the deflection of a beam in the direction of the uniaxial compression with the curvature given by Eq. 30. Thus

$$u_m = \frac{1}{8}\frac{2\varepsilon_y}{t}b^2 = \frac{1}{4}\frac{f_y}{E}\frac{b^2}{t} \tag{72}$$

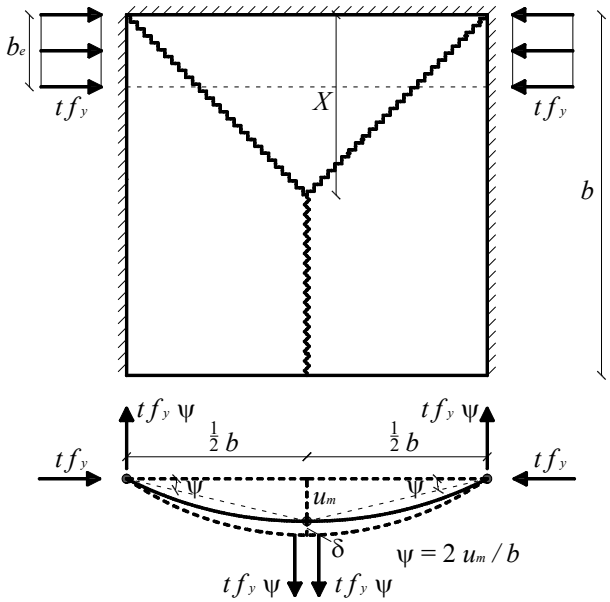

Figure 26. Failure Mechanism for a Square Plate with One Free Edge

The work equations show that the effective width is determined by:

For $b_e/b \le X/b = ½$:

$$\frac{f_y}{E}b_e^2 + \frac{t^2}{b}b_e - \frac{3}{2}t^2 = 0 \tag{73}$$

$\Rightarrow$

$$\frac{b_e}{b} = -\frac{1}{2}\lambda^{-2} + \sqrt{\frac{1}{4}\lambda^{-4} + \frac{3}{2}\lambda^{-2}} \tag{74}$$

For $b_e/b \ge X/b = ½$:

$$\left(\frac{f_y}{E}b + \frac{t^2}{b}\right)b_e = \frac{3}{2}t^2 + \frac{1}{4}\frac{f_y}{E}b^2 \tag{75}$$

$\Rightarrow$

$$\frac{b_e}{b} = \frac{\frac{1}{4}\lambda^2 + \frac{3}{2}}{\lambda^2 + 1} \tag{76}$$

In the above equations, λ is given by Eq. 35, b is the total width, t the thickness, E Young's modulus and f_y is the yield stress.

Eq. 74 and Eq. 76 are shown in Figure 27 together with the elastic buckling solution, Eq. 36, and Winter's solution, Eq. 71.

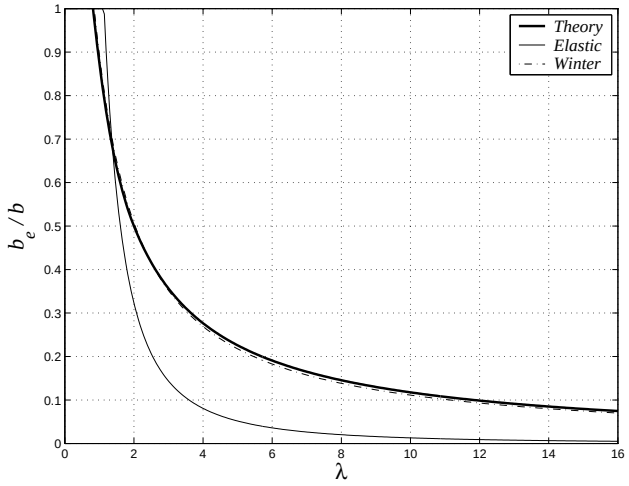

Figure 27. b_e/b as a Function of λ

Here, the buckling coefficient $k = 1.43$ is applied, cf. (Timoshenko and Gere [14]), and Poisson's ratio is taken to be $\nu = 0.30$. Again, the theoretical solution gives almost the same result as Winter's semi-empirical solution. Unfortunately, no tests have been found in the literature to verify the theory. This however is not particularly important, since square plates with one free edge are seldom used in practice.

5. IMPERFECTIONS

As previously mentioned residual stresses will have no influence on the calculations according to the theory of plasticity.

Approximately imperfections may be taken into account by adding an initial deflection to the deflection used in the above calculations. Thus it is tacitly assumed that the imperfection has the same form as the deflected shape used before.

When considering rectangular plates supported along all edges, the deflection at maximum load is determined by, cf. Eq. 31,

$$u_m = \frac{1}{4}\frac{f_y}{E}\frac{b^2}{t} + u_i \tag{77}$$

where u_i is the initial deflection, f_y the yield stress, E Young's modulus, b the total width and t is the thickness. Solving the work equation as shown in Section 3.1, leaves the result

$$\frac{b_e}{b} = \frac{-\lambda^{-2} + \sqrt{\lambda^{-4} + 4\lambda^{-2}\left(4\lambda^{-2}\frac{u_i}{t} + 1\right)}}{4\lambda^{-2}\frac{u_i}{t} + 1} \tag{78}$$

For an imperfection proportional to the thickness, the term, u_i/t, will be a constant.

Another way of taking imperfections and other unknown parameters into account is simply to introduce an empirical coefficient, μ, in the deflection formula. The deflection at maximum load

may then be written

$$u_m = \mu \frac{1}{4} \frac{f_y}{E} \frac{b^2}{t} \tag{79}$$

The effective width is found to be

$$\frac{b_e}{b} = -\frac{1}{\mu}\lambda^{-2} + \sqrt{\frac{1}{\mu^2}\lambda^{-4} + 4\frac{1}{\mu}\lambda^{-2}} \tag{80}$$

Imperfections may explain the large deviations in the tests by Sechler (Winter [15]), both from Winter's formula and the present theoretical estimate.

In Figure 25, it was shown that the tests by Sechler coincided closely with the theoretical estimate for small values of b_e/b, i.e. large values of λ, while for low values of λ, the deviation was large. For the tests by Sechler shown in Figure 25, the mean value is 1.202. By requiring the mean value 1.0 and by applying Eq. 79 to find the imperfection coefficient, $\mu = 1.52$ is found. The correlation between the tests and the theory, cf. Eq. 80, with $\mu = 1.52$ is shown in Figure 28. In this way, a smaller deviation is achieved for low values of λ, but the scatter is still large.

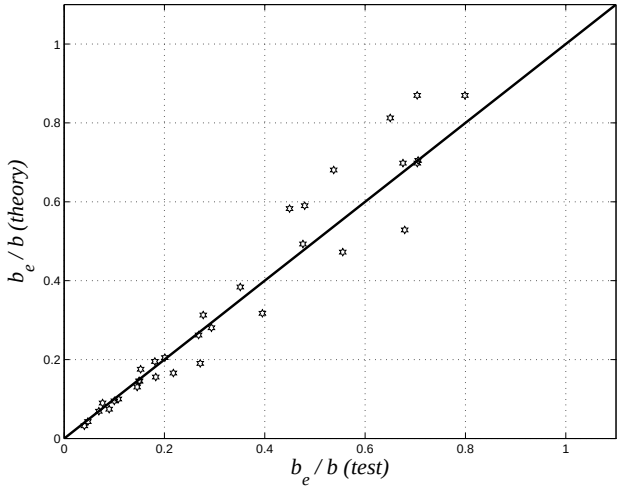

Figure 28. Theory Versus Tests for $\mu = 1.52$

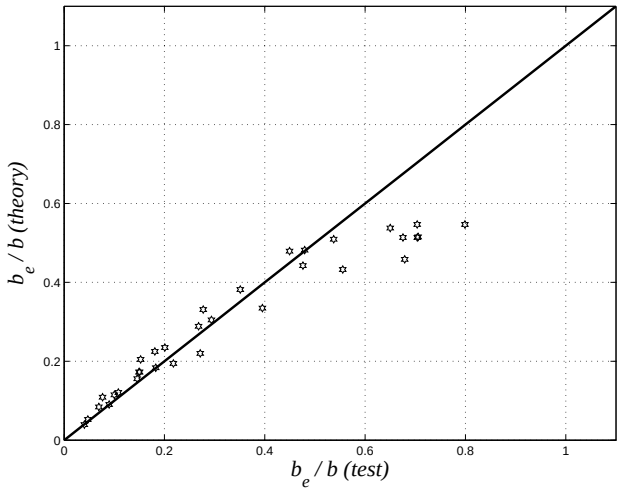

Figure 29. Theory Versus Tests for $u_i/t = 1.94$

Unfortunately, the report by Sechler [13] referred to by Winter has not yet been available to the authors. From Winter's reference it is only possible to deduce the value of λ, while the thickness of the specimens remains unknown. By applying Eq. 78 and require the mean value 1.0, $u_i/t = 1.94$ is found. The correlation between the tests and the theory with $u_i/t = 1.94$, cf. Eq. 78, is shown in Figure 29.

It appears that the effect is small for large values of λ, and large for low values of λ, which is precisely the requirement for removing the discrepancy. However, the effect on the result for low values of λ seems to be too great. Thus by applying Eq. 40, the theory overestimates the load-carrying capacity for low values of λ, while the opposite is achieved by applying Eq. 78. Hence it is not possible to verify Eq. 78 by these tests.

Apart from initial imperfections, there may of course be other explanations for the large deviations found in the Sechler tests. In tests, it is very difficult to correctly establish the ideal support conditions. The supports require the four edges of the initial mid-plane of the plate to remain in the same plane at all times. A solution was suggested by Schuman and Back [12] for the case of single plate specimens. In their tests, the specimens were, as mentioned above, supported by V-grooves, which cause any initial curvature of the edges to increase, which may again cause failure at a lower load than otherwise expected. The effect will be relatively larger for the thicker specimens. Therefore problems related to V-grooves might also explain the deviations in the Sechler tests. However, this is quite hypothetical, since at the moment it is not known if this kind of support was even used in the tests.

6. OTHER APPLICATIONS OF THE THEORY

The simple theory developed above may be extended to apply to a large number of practically important cases.

Firstly, an external lateral load may be taken into account by simply adding the work done by the lateral load to the external work, calculated as above. Further, biaxial compressive loads may be treated in the same manner without difficulties. Stiffeners and the compression flange in plate girders may be calculated by formulae given above.

Fixed supports may be treated by adding the contribution from the negative yield line at the fixed supports to the dissipation. However, the deflection at maximum load must also be changed, so that it corresponds to the fixed boundary conditions.

Considering two cases of long rectangular plates with fixed unloaded edges (one fixed unloaded edge and both unloaded edges fixed), the failure mechanisms may be as shown in Figure 30 and 31, respectively. In both cases, the plate may be subdivided into square plates as shown in the figures. Here the deflection at maximum load is given by Eq. 31. The load-carrying capacity for a plate with one fixed unloaded edge is then

$$\frac{b_e}{b} = -\lambda^{-2} + \sqrt{\lambda^{-4} + 5\lambda^{-2}} \tag{81}$$

The load-carrying capacity for a plate with both unloaded edges being fixed equals

$$\frac{b_e}{b} = -\lambda^{-2} + \sqrt{\lambda^{-4} + 6\lambda^{-2}} \tag{82}$$

Eq. 81 and 82 are shown in Figure 32 and 33, respectively. The figures also show the results determined be Winter's formulae. Again, the results presented coincide closely with Winter's formulae.

Finally, it is probably also possible to calculate in-plane bending loads. However, other mechanisms have to be used in this case.

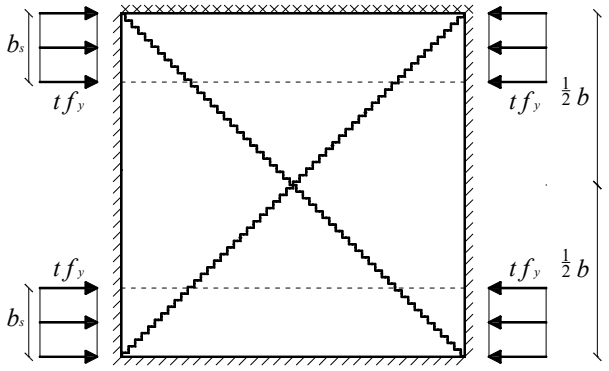

Figure 30. Failure Mechanism for a Plate with One Fixed Unloaded Edge

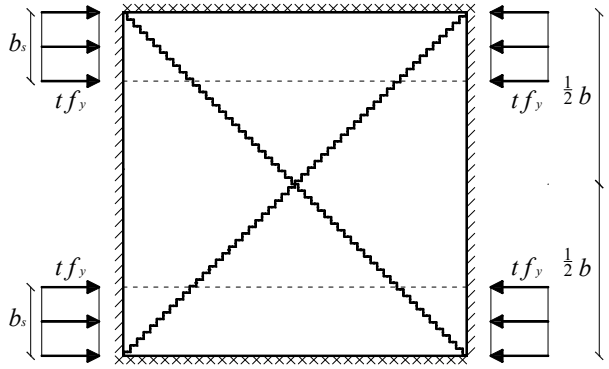

Figure 31. Failure Mechanism for a Plate with Both Unloaded Edges Fixed

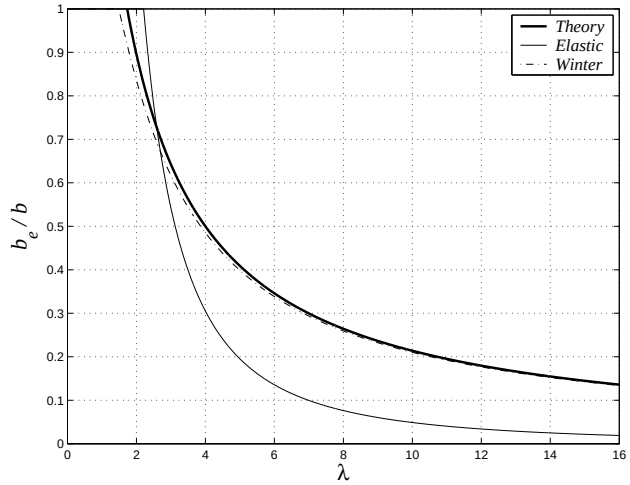

Figure 32. b_e/b as a Function of λ, Fixed Supports Along One Unloaded Edge

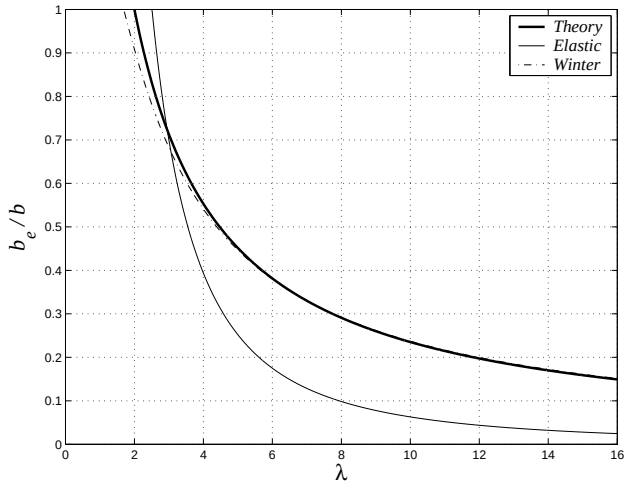

Figure 33. b_e/b as a Function of λ, Fixed Supports Along Both Unloaded Edges

7. CONCLUSION

It is shown that extremely simple estimates of the post-buckling strength of plates with in-plane loading may be obtained by using plastic solutions for the deflected shape. This shape must be known or estimated before the calculation can be carried out. It seems that useful estimates of the deflected shape may be found using simple formulae from beam theory and plate theory.

Initially, the calculation procedure is illustrated by simple solutions for columns. Solutions for plates are derived for the two practically important cases: Plates supported along all edges and plates with one free edge. In both cases, the theory is applied on both square and rectangular plates. Furthermore, it is shown how imperfections may be taken into account. Finally, it is shortly explained how the theory may be extended to a large number of other practically important cases. The results have been compared with the well-known formulae of Winter and with tests. The agreement in both cases is very good.

NOTATION

a	plate length
b	plate width
b_e	total effective width
b_s	width of effective strip
f_y	yield stress
k	elastic buckling coefficient
m	bending capacity of a yield line per unit length; fictitious moment
m_b	bending moment per unit length in a yield line
m_p	plastic yield moments per unit length
n	normal force per unit length
n_p	load-carrying capacity per unit length in pure compression or tension
m_{px}, m_{py}	plastic yield moment in the x-direction and the y-direction, respectively
p	lateral load per unit area
t	thickness
u, u_A, u_B	deflection; deflection at point A and B, respectively
u_i	deflection from imperfections

u_m	deflection at maximum load
x, y	coordinates in a Cartesian x,y -system of coordinates
A	cross-sectional area
C	empirical coefficient
E	Young's modulus
L	length
M	total moment
M_p	plastic yield moment
N	normal force
N_{cr}	critical buckling load
N_p	load-carrying capacity in pure compression or tension
W_e, W_i	external work and dissipation, respectively
X, Y	free optimisation parameters
α	parameter (shape of curvature function); imperfection factor
δ	displacement increment
ε_y	yield strain
κ, κ_{xy}	curvature and torsional curvature, respectively
λ	non-dimensional parameter
λ_r	non-dimensional slenderness ratio according to EC3
μ	empirical coefficient
ν	Poisson's ratio
σ	normal stress
σ_e	edge stress
ψ	angular deflection increment
Δ	difference
Φ	EC3 parameter for calculation of columns

REFERENCES

[1] Bambach, M.R. and Rasmussen, K.J.R., "Tests on Unstiffened Plate Elements under Combined Compression and Bending", J. Struct. Eng. ASCE, 2004, Vol. 130, No. 10, pp. 1602-1610.

[2] Bryan, G.H., "On the Stability of a Plane Plate under Thrusts in Its Own Plane, with Applications to the Buckling of the Sides of a Ship", Proc. Lond. Math. Soc. 1891, Vol. 22.

[3] European Committee for Standardisation (EC3 1993), "Eurocode 3: Design of Steel Structures – Part 1-1: General Rules and Rules for Buildings", EN 1993-1-1, Brussels: CEN.

[4] European Committee for Standardisation (EC3 2005), "Eurocode 3: Design of Steel Structures – Part 1-5: Plated Structural Elements", ENV 1993-1-5, Brussels: CEN.

[5] Hiriyur, B.K.J. and Schafer, B.W., Yield-Line Analysis of Cold-Formed Steel Members", Submitted to International Journal of Steel Structures, August 2004.

[6] Johansen, K.W., "Brudlinieteorier", Copenhagen: Gjellerup, 1943. English translation: Johansen, K.W., "Yield Line Theories", London: Cement and Concrete Association, 1962.

[7] Kalyanaraman, V., Winter, G. and Pekoz, T., "Unstiffened Compressed Elements", J. Struct. Div. ASCE, 1977, Vol. 103, No. 9, pp. 1833-1848.

[8] Kármán, T. von, Sechler, E.E. and Donnell, L.H., "The Strength of Thin Plates in Compression", Trans. ASME, 1932, Vol. 54, pp. 53-57.

[9] Moxham, K.E., "Buckling Tests on Individual Welded Steel Plates in Compression", Report CUED/C-Struct/TR.3, Cambridge: University of Cambridge, 1971.

[10] Murray, N.W., “Introduction to the Theory of Thin-Walled Structures,” Oxford: Clarendon Press, Oxford Science Publications, 1984.
[11] Nielsen, M.P., “Limit Analysis and Concrete Plasticity”, 2nd ed., Boca Raton, Florida: CRC Press, 1998.
[12] Schuman, L. and Back, G., “Strength of Rectangular Flat Plates under Edge Compression”, Technical Report No. 356: National Advisory Committee for Aeronautics, 1930.
[13] Sechler, E.E., “The Ultimate Strength of Thin Flat Sheet in Compression”, Publication No. 27, Pasadena: Guggenheim Aeronautics Laboratory, California Inst. of Technology, 1933.
[14] Timoshenko, S.P. and Gere, J.M., “Theory of Elastic Stability”, 2nd ed., New York: McGraw-Hill Book Co., Inc., 1961.
[15] Winter, G., “Strength of Thin Steel Compression Flanges”, Trans. ASCE, 1947, Paper No. 2305, Vol. 112, pp. 527-554.
[16] Zhao, X.L., “Yield Line Mechanism Analysis of Steel Members and Connections”, Structural Analysis and CAD, Prog. Struct. Engng. Mater., 2003, Vol. 5, pp. 252-262.